ARTICLE PUBLISHED AS: Scripta Materialia, Volume 172, November 2019, Pages 72-76. https://doi.org/10.1016/j.scriptamat.2019.07.006

A mechanism for basal vacancy loops formation in zirconium

C. Dai, P. Saidi, M. Topping, L. K. Béland, Z. Yao, M. R. Daymond*
Department of Mechanical and Materials Engineering, Queen's University, Kingston, ON K7L 3N6, Canada

Experiments and molecular dynamics were combined to determine a formation mechanism for basal vacancy loops in zirconium. In scanning/transmission electron microscopy images with different tilting angles, the majority of prismatic loops lying on a given basal plane do not align on a trace, but are seemingly randomly distributed in the plane. Similar arrangements are observed in molecular dynamics simulations. Over 200 collision cascade simulations were performed. Basal cascade-induced dislocation segments are observed in arrangements with a high density of prismatic vacancy loops, consistent with earlier experimental observations. This mechanism of basal loop formation may explain the observed incubation period.

Keywords: lattice defects; radiation damage; scanning/transmission electron microscopy (STEM); molecular dynamics (MD)

Zirconium alloys are important fuel-cladding and structural materials in thermal nuclear reactors [1, 2] due to their low thermal neutrons capture cross-section and reasonable corrosion resistance [3]. Irradiation-induced vacancies and self-interstitial atoms (SIAs) can stabilize themselves in the form of a vacancy or interstitial loop, respectively. However, the precise thermodynamic and kinetic conditions of this rearrangement remains to be elucidated [4]. Vacancy and interstitial clusters are important precursors for the formation of dislocation loops. These clusters can be either created directly by collision cascades or by agglomeration of point defects [2]. The dislocation loops in α-Zr with hexagonal closed-packed (HCP) crystal structure are classified as prismatic (*a*-type) or basal (*c*-component) based on their Burgers

vector. The most common experimentally measured Burgers vector of dislocation loops for a-type and c-component are $1/3\langle 11\bar{2}0\rangle$ [5] and $1/6\langle 20\bar{2}3\rangle$ [6], respectively. Formation of dislocation networks [7], brittle fracture [8], growth [9] and low creep resistance [10] are associated with the occurrence of such loops, motivating study of formation and growth of dislocation loops in Zr alloys.

Dislocation loops in α-Zr exhibit a relationship between loop type and the irradiation environment. At relatively low neutron fluences ($< 3 \times 10^{25}$ neutrons/m^2), dislocation loops are reported to be exclusively $1/3\langle 11\bar{2}0\rangle$ a-type, of both interstitial and vacancy type [5, 11-15]. However, Holt *et al*. [16] observed that in neutron-irradiated Zircaloy-2, at a fluence of 6×10^{25} neutrons/m^2, c-component loops form. As determined by Griffiths and his co-workers [6, 17-21], the majority of c-component loops are vacancy in nature. It is thus generally accepted that in Zr and its alloys, a-type loops appear at low irradiation fluences whereas c-component loops appear at higher doses [16]. Also, c-component loops are associated with and likely responsible for accelerated irradiation growth, as well as contributing to irradiation creep and degradation of mechanical properties [22]. However, the formation of c-component loops is a complex problem and finding the formation conditions and transition mechanisms from a-type to c-component can help us develop materials' design strategies to limit irradiation growth.

Varvenne *et al*. [23] determined the stability of a single vacancy cluster in pure α-Zr using an *ab initio*-based model that calculated formation energies of vacancy loops in different configurations. Their results show that a-type vacancy loops are the most stable loops, perhaps explaining why the majority of experimentally observed loops at lower fluences are *a*-type loops. As reported by Gilbert *et al* [13] and Northwood *et al* [14] after neutron irradiation, a-type vacancy loops formed parallel to each other and seem aligned to basal traces. Such loop stacking likely affects growth behavior, but a fundamental mechanism to explain this phenomenon is lacking. Recently, Harte *et al.* [24] hypothesized that a row of a-type loops aligned in a basal plane trace might collapse into a coarse c-component loop, based on a correlation between the absence of these a-loops at the position of c-loops. They proposed that c-loop

formation requires a minimum concentration of well-aligned a-loops; this hypothesis could explain the delayed onset of c-loop nucleation.

The goal of the present study is to use experiments and atomistic simulations to explore a formation mechanism of c-loops, and to understand the relationship between a-loops and c-loops. This is done in three steps. First, the arrangement of a-loops in a basal plane from proton irradiation are clarified by a transmission electron microscopy (TEM) tilt series. Second, the stability of aligned a-loops is investigated by molecular dynamics (MD) simulations, including a stress field analysis during loop repulsion in pure Zr. Third, the formation of *c*-loops via the interaction of collision cascades with a-loops is assessed, based on 200 MD runs. Early experiments by Griffiths *et al*. [25] on neutron-irradiated Zr show that most dislocation loops near grain boundaries are vacancy type. Moreover, recent MD work [26] reported that more vacancies remain near grain boundaries after cascades, which may enhance vacancy loop formation. For MD simulations in this work, it is thus assumed that there is a local concentration of *a*-type vacancy loops, and thus only *a*-type vacancy loops are considered in the initial conditions.

TEM was carried out on a proton-irradiated Zircaloy-2 specimen. The sample was proton-irradiated at 3 MeV at 573 K with a current density of 0.1 $\mu A/mm^2$ to a damage level of 0.02 dpa. High angle annular dark field (HAADF) images were taken on a FEI OSIRIS at 200 kV with a probe current of 0.63 nA. The images were taken around the $\langle 10\bar{1}0 \rangle$ zone axis to view the a-type loops perpendicular to their habit plane.

The spatial distribution of a-type loops may affect their growth behavior and potentially relate to the formation of c-component loops, as previously hypothesised [24]. While it has been observed that a-type loops may align to the trace of the basal plane [13, 14], the alignment *direction* is unclear. To clarify the arrangement within the basal plane, we carried out a tilt series. This involved tilting along the $\langle 11\bar{2}0 \rangle$ direction, starting at the $\langle 10\bar{1}0 \rangle$ zone axis, to observe any alignment within the basal plane trace. Figure 1 shows a series of HAADF scanning/transmission electron microscopy (STEM) images with different tilting angles. Despite the apparent strong alignment of loops suggested in Figure 1 (a), in fact most a-

type loops are relatively randomly distributed within the basal plane (*i.e.*, through foil thickness). There are a few loops aligned in the same direction, as indicated by white arrows. This experimental observation provides an important guidance to the setup of our MD simulations. A sample was also irradiated at a higher irradiation dose of 1.0 dpa, but it was impossible to identify the loops arrangement in a tilt series due to the overlapping strain fields. A more detailed discussion is presented in the Supplementary materials.

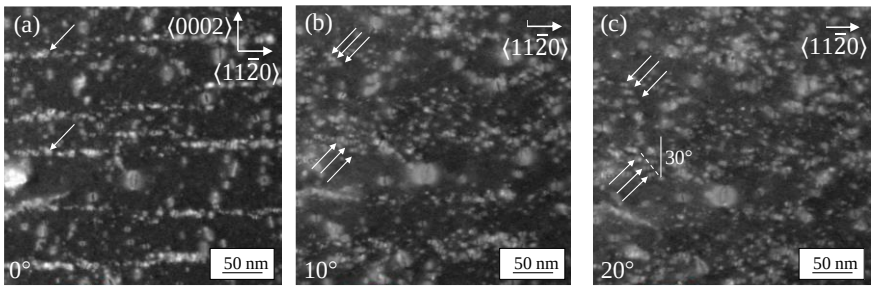

Figure 1. A tilt series of HAADF STEM image starting from the $\langle 10\bar{1}0 \rangle$ zone axis and tilting along the $\langle 11\bar{2}0 \rangle$ direction, towards the $\langle 0002 \rangle$ zone axis. The white arrows highlight the same set of *a*-loops through each tilt, highlighting a rare case of *a*-loops aligning with parallel habit planes. a) HAADF image taken on the $\langle 10\bar{1}0 \rangle$ zone axis. b) 10° tilt along the $\langle 11\bar{2}0 \rangle$ direction. c) 20° tilt along the $\langle 11\bar{2}0 \rangle$ direction.

MD simulations were performed using LAMMPS (Large-scale Atomic/Molecular Massively Parallel Simulator) [27]. The MA07[28] Zr potential (#3) was selected for the cascade simulations as this potential captures important features to simulate dislocation loops, such as adequate stacking fault energies [23]. It has been used in recent simulations [29-33]. Vacancy loops of sizes 8 nm to 10 nm in diameter are considered in this work, and the number of total atoms is 4 million. The method used to create dislocation loops in MD is in previous publications [32, 33]. Annealing using MD was performed for at least 1 ns in the NPT ensemble. All cascade simulations were carried out at 573 K, a common temperature during neutron irradiation [3]. The cascade simulations were performed in the NVE ensemble with a variable timestep. All MD simulations are under periodic boundary conditions. Images of atomic configurations were produced with OVITO (Open Visualization Tool) [34], and the crystal structure identified by common neighbor analysis [35].

Figure 2 (a) shows three parallel a-type vacancy loops at 8 nm separation as the simulation begins; all loops are 8 nm in diameter. During thermal annealing at 573 K, the three loops repel each other. The geometry of dislocation loops is such that a stress field analysis is more easily performed in a cylindrical coordinate system; see [36] for more detail. The axial-direction stress component (S_{AD}) was calculated to analyze the tilting tendency of the repulsive loops; positive stress is tensile, and negative is compressive. The stress components of each a-type vacancy loop are presented on the right-hand side of each figure in Figure 2 (b-d). A correlation time of 0.1 ps was used to generate 10 independent snapshots for the statistical analysis of the stress field around the loop. Figure 2 shows the position and S_{AD} of three a-type vacancy loops at different times. At 200 ps in Figure 2 (b), S_{AD} around the outside of the middle loop is under compression since the two loops are very close on both sides. With such stress field information, the tilting tendency of these three loops can be predicted: the middle loop would mainly rotate without much gliding since it has compression on both sides of the loop; the lower and upper loops would both rotate and glide away from their original positions since the area of compression is larger than that of tension. While in isolation the stress state inside a vacancy loop is expected to be tension [36], the stress inside these three loops is less uniform and more complicated. At 300 ps in Figure 2 (c), the separation distance between the three loops increases, and the movement of each loop is in good agreement with the qualitative prediction above. In addition, all vacancy loops now show tension inside each loop; also the magnitude of the compression outside of the loops decreases, which indicates that the tendency for the loops to further tilt has decreased. At 500 ps in Figure 2 (d), S_{AD} for the lower and the upper loops has returned to a relaxed state, but there is still some residual tensile stress around the middle loop. At 900 ps in Figure 2 (e), all the loops are in a relaxed state. The three loops in the MD simulations share the same basal plane (viewed along the *x*-axis direction), which is similar to the loops distribution observed in Figure 1 (a). However, the three loops are *not* centered about a common line (viewed along the *z*-axis direction in Figure 2 (e)), which is exactly consistent with the experimental observations in Figure 1 (b-c) and in contrast to previously assumed arrangements. This MD simulation suggests that the total energy of

multiple interacting loops is lower when loops are randomly distributed rather than perfectly aligned, which is supported by an elasticity-based model presented in the Supplementary materials.

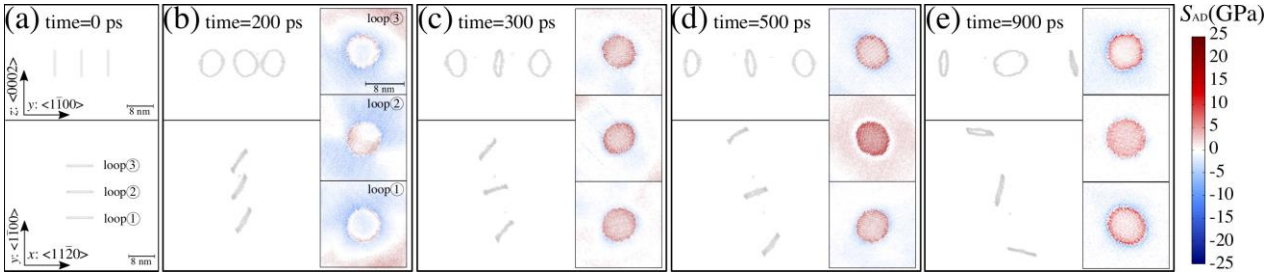

Figure 2. The evolution of three *a*-type vacancy loops repulsion during thermal annealing at 573 K. (a) The three loops are separated by 8 nm at the beginning. (b-e) Atomic configurations of the three loops on the left-hand side at 200 ps, 300 ps, 500 ps and 900 ps, respectively, in two different view projections. The three pictures shown on the right-hand side are the axial-direction component of stress (S_{AD}) for the corresponding three *a*-type vacancy loops. S_{AD} is tension in red and compression in blue.

Recent experiments [24] suggest that *c*-loop formation is related to the alignment of pre-existing *a*-type loops. The STEM images presented in this work further indicate that the majority of loops of the same basal plane are not aligned, but are arranged in a "basal-disk-like" configuration. Since the habit plane of *c*-component vacancy loops is the basal plane, the existence of *c*-component vacancy loops requires a high planar density of vacancies in the basal plane; a "basal-disk-like" configuration of *a*-type vacancy loops naturally provides exactly this. We expect disk-like arrangements to favor *c*-component loop formation, relative to arrangements along a straight line. MD cascade simulations were therefore carried out in the vicinity of *a*-type vacancy loops in various different arrangements. Table I shows the probability of forming *c*-component vacancy loops under different scenarios. From a total of 200 cascade simulations, the highest probability to form *c*-component vacancy loops is the case where one 50 keV primary knock-on atom (PKA) interacts with 11 *a*-type vacancy loops. Prior to the cascades, the arrangement of the 11 *a*-type vacancy loops on the *x*-*y* (basal) plane is shown in Figure 3 (a). The loops are all in the same basal plane but not all aligned, as guided by the above discussion. Here we illustrate one result in detail to show the formation of a *c*-component dislocation loop from the interactions of one 50 keV PKA with 11 *a*-type

vacancy loops. During the collision cascades, some pre-existing a-type vacancy loops in Figure 3 (a) collapsed into a larger vacancy loop. Figure 3 (b) depicts the results showing a newly formed small *c*-component dislocation loop near a large *a*-type vacancy loop. This small loop was determined as vacancy in nature by Wigner Seitz analysis [37-39], and further identified as *c*-component, with a Burgers vector of $1/6\langle 20\bar{2}3\rangle$. A detailed verification is provided in the Supplementary materials. The size of all newly formed *c*-component vacancy loops is about 3~4 nm in diameter. This cascade-induced change in the Burgers vector of dislocation loops is similar to that observed by Granberg *et al*. [40] in bcc Fe. Figure 3 (c) shows high magnification of the atomic structure of the c-loop, which has a pyramidal shape due to its associated stacking faults.

Table I. The probability of forming *c*-component vacancy loops ($P^{\mathrm{F}}_{c-\mathrm{loop}}$) in different irradiation environments in various conditions.

PKAs condition	Irradiation environment	$\rho^{\mathrm{ND}}_{a-\mathrm{loop}}$ ($\times 10^{22}$ m^{-3})	$P^{\mathrm{F}}_{c-\mathrm{loop}}$
One 10 keV PKA	Perfect Zr matrix	0	0/8
	1 *a*-type vacancy loop	1.07	0/17
	3 *a*-type vacancy loops	3.22	0/25
	11 *a*-type vacancy loops	11.8	1/20
Eighteen 1 keV PKAs	1 *a*-type vacancy loop	1.07	0/20
	2 *a*-type vacancy loops	2.15	1/30
One 50 keV PKA	Perfect Zr matrix	0	0/11
	1 *a*-type vacancy loop	1.07	0/30
	7 *a*-type vacancy loops	7.51	2/19
	11 *a*-type vacancy loops	11.80	5/20

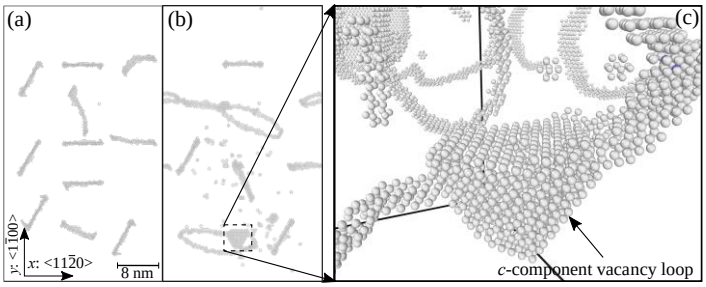

Figure 3. (a) 11 *a*-type vacancy loops with diameter of 8 nm, initially relaxed at 573 K. (b) Atomistic configurations after a one 50 keV cascades at 573 K. (c) Enlarged view showing the atomic structure of a *c*-component vacancy loop. Only displaced atoms are shown here based on common neighbor analysis.

Based on the statistical results in Table I and the TEM work in this study and others, two important factors appear to control the formation of *c*-component vacancy loops during irradiation: the kinetic energy of the PKA and the number density of *a*-type vacancy loops.

Low-dose irradiation forms predominantly *a*-type loops, as discussed above; the density of *a*-type loops increases with dose. As noted above, *c*-component loops only form above a threshold dose, e.g., Harte *et al.* [24] observed that *c*-component loops formed at a dose of 7.0 dpa. We see that cascade-induced *c*-loops are absent in simulation volumes containing a low density of *a*-type vacancy loops, and only form in simulation volumes containing a high density of *a*-type vacancy loops, providing a clear mechanism to explain why *c*-loops require an incubation period before nucleation.

Experimentally, *c*-component loops form in volumes where *a*-type loops previously lay in the same basal plane [24, 41]. The *a*-type loop number density ($\rho^{\mathrm{ND}}_{a-\mathrm{loop}}$) increases as dose increases, ranging from 0.5 $\times 10^{22}$ m^{-3} to ~ 3 $\times 10^{22}$ m^{-3} [24, 41]. This corresponds to center-to-center distance of 5-10 nm. An interesting point is that this is the approximate dimension of the volume affected by a 10 keV destructive supersonic shockwave (see Ref. [42] for an illustration), an energy close to the threshold energy of cascade fragmentation [43]. In other words, cascade overlap with pre-existing microstructure is likely to play a key role. In atomistic simulations, *c*-component vacancy loops can be obtained by artificially removing vacancy platelets in the basal plane [23, 44, 45]; thus, a high local density of vacancies is essential to form

c-component vacancy loops. From the MD study here, $P^{\mathrm{F}}_{c-\mathrm{loop}}$ is the highest when $\rho^{\mathrm{ND}}_{a-\mathrm{loop}}$ is the highest too, because a high density of *a*-type vacancy loops in a basal plane increases the local vacancy density.

High-energy collision cascades provide opportunities to reach states well out-of-equilibrium, which would be thermodynamically or kinetically suppressed in other circumstances. Notably, they interact with pre-existing structures via (super-)sonic shockwaves [46, 47], thermal spikes [48] and point defect production [49, 50]. Our MD simulations are limited to nano-second time scales; it is difficult to simulate the full growth process of these small *c*-loops. We however aged the *c*-loops for up to 30 ns at 573K. Two of the small *c*-loops were stable and the others were lost due to the interactions with the surrounding defects, as further explained in the Supplementary materials. We can expect that – based on various rate theories [9, 51-53]– that vacancy type *c*-loops will grow with time. An interesting point is that one such rate theory [52, 53] *assumes* a critical radiation dose for nucleation of vacancy type *c*-loops. The present study provides evidence that supports this assumption, however, our results indicate that in contrast to the rate theory assumptions, the *c*-component vacancy loops begin to form due to the collapse of *a*-type vacancy loops rather than from the accumulation of individual vacancies. Adaptive Monte Carlo methods, such as the kinetic Activation Relaxation Technique [54] or the Self-Evolving Atomistic Kinetic Monte Carlo [55] are able to reach the long times needed to study the transformation of dislocation loops [56-58]. Extending the work presented here with a long-time scale computational method would be valuable, e.g., the interaction of *a*-type and *c*-component loops on long timescales would be of great interest. These types of simulations could bridge a missing link: our simulations reveal very small *c*-loops, while large *c*-loops are typically seen experimentally. They may help identify a hypothetical critical *c*-loop size. In addition, the effect of *a*-type interstitial loops on the formation of *c*-component vacancy loops is not clear, and it would be of interest to study how the populations of vacancy and interstitial *a*-type loops evolve over time. More generally, our work highlights the necessity for future predictive models to consider the nucleation of *c*-loops from pre-existing vacancy *a*-type loops. This mechanism is currently missing from the existing rate

theory models, highlighting the benefits of using multiple techniques to study complex phenomena such as irradiation damage.

In conclusion,

i) the arrangement of a-type loops in a basal plane from proton irradiation have been clarified by TEM and further explained by MD simulations: most a-type loops are relatively randomly distributed within a basal plane. That is, while they do lie on a basal plane they are not linearly aligned. A good agreement between the TEM and MD techniques was achieved.

ii) Using atomistic simulations, cascade-induced c-component vacancy loops were observed—to our knowledge—for the first time. They arise from the interaction between a cascade and a dense cluster of pre-existing a-type vacancy loops in a basal plane. This is consistent with our own experimental observations and those in the literature. This finding is key to understanding the formation of c-component loops, and the presence of a nucleation period before they form.

The authors thank Compute Canada for access to computing resources. The research was supported by NSERC and the NSERC/UNENE Industrial Research Chair in Nuclear Materials at Queen's.

References

[1] R.A. Holt, J. Nucl. Mater. 372(2–3) (2008) 182-214.
[2] G.S. Was, Fundamentals of Radiation Materials Science: Metals and Alloys, Springer Berlin Heidelberg2007.
[3] F. Onimus, J.L. Béchade, in: R.J.M. Konings (Ed.), Comprehensive Nuclear Materials, Elsevier, Oxford, 2012, pp. 1-31.
[4] S.J. Zinkle, G.S. Was, Acta Mater. 61(3) (2013) 735-758.
[5] P.M. Kelly, R.G. Blake, Philos. Mag. 28(2) (1973) 415-426.
[6] M. Griffiths, M.H. Loretto, R.E. Smallman, J. Nucl. Mater. 115(2–3) (1983) 323-330.
[7] A. Iyad Alabd, J.R. Carlos, G. Yu, M.U. Herbert, Nanotechnology 27(4) (2016) 045706.
[8] M.A.L. De Oliveira, G. Michot, Acta Mater. 46(4) (1998) 1371-1383.
[9] R.A. Holt, J. Nucl. Mater. 159 (1988) 310-338.

[10] F.A. Garner, M.B. Toloczko, B.H. Sencer, J. Nucl. Mater. 276(1) (2000) 123-142.
[11] R.B. Adamson, W.L. Bell, D. Lee, American Society for Testing and Materials, STP 551(551) (1974) 215-228.
[12] D.O. Northwood, V. Fidleris, R.W. Gilbert, G.J.C. Carpenter, J. Nucl. Mater. 61(2) (1976) 123-130.
[13] R.W. Gilbert, K. Farrell, C.E. Coleman, J. Nucl. Mater. 84(1–2) (1979) 137-148.
[14] D.O. Northwood, R.W. Gilbert, L.E. Bahen, P.M. Kelly, R.G. Blake, A. Jostsons, P.K. Madden, D. Faulkner, W. Bell, R.B. Adamson, J. Nucl. Mater. 79(2) (1979) 379-394.
[15] A. Jostsons, P.M. Kelly, R.G. Blake, J. Nucl. Mater. 66(3) (1977) 236-256.
[16] R.A. Holt, R.W. Gilbert, J. Nucl. Mater. 116(1) (1983) 127-130.
[17] M. Griffiths, M.H. Loretto, R.E. Smallman, J. Nucl. Mater. 115(2–3) (1983) 313-322.
[18] M. Griffiths, R.W. Gilbert, J. Nucl. Mater. 150(2) (1987) 169-181.
[19] M. Griffiths, D. Gilbon, C. Regnard, C. Lemaignan, J. Nucl. Mater. 205 (1993) 273-283.
[20] M. Griffiths, R.C. Styles, C.H. Woo, F. Phillipp, W. Frank, J. Nucl. Mater. 208(3) (1994) 324-334.
[21] Y.d. Carlan, C. Regnard, M. Griffiths, D. Gilbon, C. Lemaignan, Zirconium in the Nuclear Industry: Eleventh International Symposium, STP16194S, E. Bradley and G. Sabol, Ed., ASTM International (1996) 15.
[22] F. Long, L. Balogh, D.W. Brown, P. Mosbrucker, T. Skippon, C.D. Judge, M.R. Daymond, Acta Mater. 102 (2016) 352-363.
[23] C. Varvenne, O. Mackain, E. Clouet, Acta Mater. 78 (2014) 65-77.
[24] A. Harte, D. Jädernäs, M. Topping, P. Frankel, C.P. Race, J. Romero, L. Hallstadius, E.C. Darby, M. Preuss, Acta Mater. 130 (2017) 69-82.
[25] M. Griffiths, R.W. Gilbert, C.E. Coleman, J. Nucl. Mater. 159 (1988) 405-416.
[26] J.E. Ludy, T.J. Rupert, Scripta Mater. 110 (2016) 37-40.
[27] S. Plimpton, J. Comput. Phys. 117(1) (1995) 1-19.
[28] M.I. Mendelev, G.J. Ackland, Philos. Mag. Lett. 87(5) (2007) 349-359.
[29] S. Di, Z. Yao, M.R. Daymond, F. Gao, Nucl. Instrum. Methods Phys. Res., Sect. B 303 (2013) 95-99.
[30] S. Di, Z. Yao, M.R. Daymond, X. Zu, S. Peng, F. Gao, Acta Mater. 82 (2015) 94-99.
[31] K. Ghavam, R. Gracie, J. Nucl. Mater. 462 (2015) 126-134.
[32] C. Dai, L. Balogh, Z. Yao, M.R. Daymond, Philos. Mag. (2017) 1-13.
[33] C. Dai, L. Balogh, Z. Yao, M.R. Daymond, J. Nucl. Mater. 478 (2016) 125-134.
[34] S. Alexander, Modell. Simul. Mater. Sci. Eng. 18(1) (2010) 015012.
[35] D. Faken, H. Jónsson, Computational Materials Science 2(2) (1994) 279-286.
[36] C. Dai, P. Saidi, Z. Yao, M.R. Daymond, Acta Mater. 140 (2017) 56-66.
[37] K. Nordlund, M. Ghaly, R.S. Averback, M. Caturla, T. Diaz de la Rubia, J. Tarus, Phys. Rev. B 57(13) (1998) 7556-7570.
[38] F. Gao, W.J. Weber, Phys. Rev. B 66(2) (2002) 024106.
[39] K. Nordlund, R.S. Averback, Phys. Rev. B 56(5) (1997) 2421-2431.
[40] F. Granberg, J. Byggmästar, A.E. Sand, K. Nordlund, EPL (Europhysics Letters) 119(5) (2017) 56003.
[41] E. Francis, R.P. Babu, A. Harte, T.L. Martin, P. Frankel, D. Jädernäs, J. Romero, L. Hallstadius, P.A.J. Bagot, M.P. Moody, M. Preuss, Acta Mater. (2018).
[42] L.K. Béland, Y.N. Osetsky, R.E. Stoller, Npj Computational Materials 2 (2016) 16007.
[43] A. De Backer, C. Domain, C.S. Becquart, L. Luneville, D. Simeone, A.E. Sand, K. Nordlund, J. Phys.: Condens. Matter 30(40) (2018) 405701.
[44] V.G. Kapinos, Y.N. Osetsky, P.A. Platonov, J. Nucl. Mater. 195(1) (1992) 83-101.
[45] N. de Diego, Y.N. Osetsky, D.J. Bacon, J. Nucl. Mater. 374(1–2) (2008) 87-94.
[46] A.F. Calder, D.J. Bacon, A.V. Barashev, Y.N. Osetsky, Philos. Mag. 90(7-8) (2010) 863-884.
[47] L.K. Béland, Y.N. Osetsky, R.E. Stoller, Acta Mater. 116 (2016) 136-142.
[48] T.D. De La Rubia, R.S. Averback, R. Benedek, W.E. King, Phys. Rev. Lett. 59(17) (1987) 1930.
[49] R.E. Stoller, J. Nucl. Mater. 233-237 (1996) 999-1003.

[50] R.E. Stoller, in: R.J.M. Konings (Ed.), Comprehensive Nuclear Materials, Elsevier, Oxford, 2012, pp. 293-332.
[51] C.H. Woo, J. Nucl. Mater. 159 (1988) 237-256.
[52] A.V. Barashev, S.I. Golubov, R.E. Stoller, J. Nucl. Mater. 461 (2015) 85-94.
[53] S. Golubov, A. Barashev, A. Barashev, R. Stoller, B. Singh, Breakthrough in Understanding Radiation Growth of Zirconium2015.
[54] N. Mousseau, L.K. Béland, P. Brommer, F. El-Mellouhi, J.-F. Joly, G.K. N'Tsouaglo, O. Restrepo, M. Trochet, Computational Materials Science 100 (2015) 111-123.
[55] H. Xu, R.E. Stoller, L.K. Béland, Y.N. Osetsky, Computational Materials Science 100 (2015) 135-143.
[56] H. Xu, R.E. Stoller, Y.N. Osetsky, D. Terentyev, Phys. Rev. Lett. 110(26) (2013) 265503.
[57] L.K. Béland, Y.N. Osetsky, R.E. Stoller, H. Xu, J. Alloys Compd. 640 (2015) 219-225.
[58] L.K. Béland, Y.N. Osetsky, R.E. Stoller, H. Xu, Computational Materials Science 100 (2015) 124-134.